

Model Tests on Determining the Effect of Various Geometrical Aspects on Horizontal Impedance Function of Surface Footings

Jafar Maleki^{1a*} and Fardin Jafarzadeh²

¹ MSc of Geotechnical Eng., Sharif University of Technology, Dept. of Civil Eng., Tehran, Iran

² Ph.D., Associate Professor, Sharif University of Technology, Dept. of Civil Eng., Tehran, Iran

Abstract: Problems associated with soil-structure interaction have been determined and the Impedance Functions evaluated. The aim of this paper is studying horizontal impedance function for surface footings by physical model tests. For this purpose, a cubic steel container was used as a testing environment for two different conditions, a rigid base, and a homogeneous half-space model. The effect of various parameters such as footing shape, embedment ratio, inertia, and dynamic force amplitude was studied in three shapes; rectangular, square, and circle footing. The results indicated that the massless impedance function theory was confirmed at the Dimensionless Frequency of less than 2.5. Also, in the rigid base model, soil response heavily depends on the vibration frequency, developed by boundary conditions and side walls, in contrast to the half-space model. The rigid base, distribution and reflection of waves in the soil, and dissipation of higher wave energy substantially influenced the dynamic response of soil–foundation system. Additionally, the embedment ratio significantly affected the impedance functions.

Keywords: Horizontal impedance function; Physical modeling; Dynamic response; Soil-foundation interaction; Harmonic loading; Footing vibration.

* Corresponding Author, e-mail address: jafarmaleki@alum.sharif.edu, jfmaleki22@gmail.com, Phone number: +98-21-22080191

Co-author e-mail address: fardin@sharif.edu, Phone number: +98-21-66164226

^a Present address: Geotechnical Engineer and Data Analyzer, Abgeer Consulting Engineers Company, Saadat Abad, P.BOX: 1998194655, Tehran, Iran.

1. Introduction

Dynamic loading on shallow foundations and their responses is an essential subject in the soil-structure-interaction analysis. One of the key differences between static and dynamic loading conditions is changes in some basic parameters in the soil under time-dependent loads. For example, stiffness and shear modulus of soil while applying dynamic loading is affected by the type of load, soil type, etc. Repeated loading on structures and their reaction on the foundation will cause a dynamic interaction, in particular a kind of initial interaction between subsoil and the foundation. Generated waves will propagate in soil-foundation interface, and affect soil particles. The energy of these waves in the soil medium depends on the soil type, unit weight, layout, loading type, frequency, etc.

Despite studies on effects of dynamic loading on soil, there is a general lack of proper understanding of the actual behavior complexity of soil, three-dimensional nature of wave propagation, and changes in soil's shear modulus [1]. The analysis of the force-displacement relation of a surface foundation is necessary for dynamic analysis of the machine's foundation vibrations. Investigation of the Impedance Functions (**IFs**) is necessary in the dynamic analysis of machine foundations, which predicts the dynamic motions of a foundation [2].

In designing machine foundations, it is necessary to control criteria of allowable bearing capacity and maximum settlement, since the machine resting on a foundation must work continuously and properly. Other goals in designing machine foundations are to limit the vibration of foundation while not posing any risk and preventing the resonance phenomenon of the soil-foundation system, which requires accurate detection of the resonant frequency of the system including foundation, machine, and soil. Developments in seismic testing methods and improved electronic recording capabilities have reached a level that allows computation and verification of dynamic **IFs** predictions for shallow foundations [3].

One major issue in dynamic analysis methods of a machine foundation is the prediction of the dynamic **IFs** as a function of the excitation frequency. Using this approach, the dynamic response of a foundation, e.g. the final displacement of a foundation under dynamic loadings, can be obtained at different frequencies and inertias.

In recent years, a large and growing body of literature has examined numerical methods to predict the response of shallow foundations to harmonic and seismic loadings. These numerical models are based on finite element methods, cone model method, mathematical methods, and mass-spring-damper system method. In these methods, the dynamic force-displacement relation is taken according to the soil modeling and surroundings boundary conditions by equivalent components of soil parameters on surface foundations [4-29].

Meanwhile, studies evaluating the **IFs** of structures resting on pile foundations significantly numerically and experimentally have increased. These studies have been conducted to predict the response of the pile-structure exposed to seismic excitations and harmonic loadings for a wide range of structures and frequencies [30-42].

Large-scale experiments are performed for assessing the **IFs** of surface foundations. The main advantage of the large-scale experimental method is the real conditions of the soil environment, an in turn precise simulation. Typically, the large-scale testing results are the best data for verifying numerical modeling [43-47].

Nowadays, multiple numerical models are available based on the Elasto Dynamic theories for predicting dynamic responses of foundations. It seems that these numerical models are compatible with each other and with both large- and small-scale test results [14, 15, 48-50].

However, there are limited studies conducted on small-scale experiments. As the examples are Nii [51], Wong and Luco [52] and Momeni et al. [53] who carried out an extensive investigation on **IFs** of a rigid rectangular surface foundation under viscoelastic homogeneous half-space conditions.

Although few experimental studies have confirmed the compatibility between the theoretical and numerical results, these empirical pieces of research are very limited for various reasons. Decades of research have shown significant advancements in both laboratories and in-situ characterization of geotechnical sites, and in methodologies for predicting the dynamic behavior of shallow foundations. Drawing on full-scale experimental research, Fry [54] carried out a full-scale test. Due to a lack of adequate geophysical studies to characterize the soil conditions, dynamic properties of the site were sparse, and the accuracy of data can be questioned in these experiments. Dobry et al. [55], Crouse et al. [56], Luco and Wong [57], Gazetas and Stokoe [58], and De Barros and Luco [59] studied the **IFs** on large scale testing. They applied dynamic loading on actual shallow foundations and discovered dynamic **IFs**. Also, Stokoe and Richart [60] had some model tests for considering the effect of footing shape and embedment ratio on **IFs**.

Some studies have evaluated **IFs** using physical model tests. A few important studies have been performed in this regard on surface foundations by Erden [61], Nii [51], Pak and Guzina [1], Cheney et al. [44], Fattah et al. [62] and Momeni et al. [53]. In these studies, a surface footing was placed in a container box, and a dynamic load was applied to it. Then, by recording system responses and a suitable approach, **IFs** were calculated. Because of the complexity of the analysis process through a pair of horizontal and rotational vibration modes, in previous research, a vertical vibration load was applied to the footing.

In this research, **IFs** of surface foundation were studied by applying a cyclic horizontal load using a physical model. After the calibration tests, the Babolsar sand was used. The relative unit weight of the soil model was discovered to be 54.4% through the sand raining method. A horizontal harmonic loading (created in a combination of an amplifier, a generator and a shaker) with a specific domain and frequency was employed through a generator to stimulate the mandatory foundation oscillation. Also, three different footing shapes; rectangular, square, and circle were studied. The soil-foundation system responses were

recorded using the mechanical impedance measurement technique. Employing appropriate motion equations, geometric parameters, and recorded data, dynamic **IFs** for horizontal vibration were calculated, and graphs presented the results against Dimensionless Frequency (**DF**). In this paper, the effects of footing shape, embedment ratio, dynamic loading domain, footing inertia, and dynamic moment amplitude have been investigated on the dynamic impedance function.

2. Tests program

2.1. Soil

In the present study, uniform sand called "Babolsar" sand was used after cleaning and drying. This natural sand was transported to the laboratory from the coastal city of Babolsar in the Caspian Sea. This soil, according to the USCS standard, is classified as SP. Babolsar sand particle-size distribution curve is displayed in Figure 1. Based on the standard experiments, the minimum and maximum dry unit weight of the Babolsar sand is 15.45 (kN/m³) and 17.8 (kN/m³), respectively. The soil properties are presented in Table 1.

{Insert Figure 1}

{Insert Table 1}

2.2. Container box and sand raining method

The experiments were performed in a steel container box creating a physical model with a semi-infinite half-space condition. The container had a square base with 1*1*0.8 m³ dimensions. Using the sand raining method, uniform unit weight sand soil was poured into a steel container. The relative unit weight of the model was controlled based on the pouring height and the sieve opening size [63]. The soil was prepared in layers and resembled the condition of soil layers in nature. In this study, air pluviation technique was used, and sand was dropped from 70 cm height by a sieve with opening sizes of 6 mm and formed layers with a thickness of 5 cm making a soil with relative unit weight of 54.4%. Through calibration tests, the relative unit weight of samples was adjusted. The calibration test results

are shown in Figure 2. For the calibration test, cylindrical dishes were placed on the soil surface, and sand raining was done.

To prevent wave reflection and potential errors, a 10 cm layer of sawdust (a material with high damping) was used as a damper. Table 2 reports the sawdust properties. Erden [61] stated that the sawdust can well function as an energy absorbent. Likewise, Rajabnezhad [64] compared the performance of plastof foam placed all-around of container walls with that of the sawdust and found that the sawdust outperformed plastof foam. The sawdust was placed between soil and container. For separation, a wooden frame by a thin plastic layer (0.1 mm) was placed all around the container. Rajabnezhad [64] examined different values of the plastic layer thickness and the wooden frame pattern. Finally, use of a wooden frame by a thin plastic layer presented a proper performance. A 20 cm layer of sawdust was used to simulate semi-infinite conditions and was placed in the floor of the container. A concrete slab with a thickness of 15 cm was placed at the bottom of the container to emulate the bedrock conditions.

{Insert Figure 2}

{Insert Table 2}

2.3. Footing

Three different footing shapes: square, circle, and rectangle with $L/B=2$, were used in this research (Table 3). The dimensions were chosen such that the footing was protected against slipping. The foundation was joined to a steel column with a height of 20 cm, and it was connected to the signal generators, as shown in Figure 3.

{Insert Figure 3}

{Insert Table 3}

2.4. Signal generator, shaker, and instruments

After preparation of the soil-foundation system, the footing and column were placed on the center of soil surface. Next, a loading system consisting of a shaker, metal rod, harmonic signal generator, and an amplifier was connected to the model. The shaker received a

horizontal harmonic signal generated by the signal generator from the amplifier. The signal passed through the metal rod and finally transmitted to the column. The model and the loading system are shown in Figure 4.

The metal rod was used to prevent excessive soil disturbance, and the load was applied to the footing in a horizontal direction. This rod was designed and made in a way that the axial to lateral stiffness ratio helped transfer as much load as possible in the axial direction [66]. As shown in Figure 4, the shaker was placed on top of the container, and the metal rod was connected to column in a horizontal direction.

The frequency range was chosen as 50-450 Hz for dynamic response of various types of structures to harmonic loadings of actual machines. It included the frequency limits of large foundations, e.g. turbines, large silos, as well as large and relatively rigid footings in power plants. The loading duration was 16 seconds consisting of sinusoidal harmonic cycles at a specific frequency. Also, 20 Hz steps were used for tests as uniform intervals. The force magnitude was recorded by an installed load cell located at the column and the metal rod crossing. The rectangular footing was placed in the direction of the longer side under horizontal harmonic loading to compare the effects of the shape on the dynamic response. Further, the movement in the horizontal direction was captured by an accelerometer installed in the horizontal direction (the same force direction).

{Insert Figure 4}

3. Physical model properties

The soil medium was made repeatedly, with the same relative unit weight. Two accelerometers were installed into soil 0.4 m apart from each other vertically, to measure the pressure velocity of the wave through the soil model. One footing was set on the soil model, and body waves were generated using a specific hammer, in vertical direction. Employing the data of two sensors, the time delay between the arrival times of the waves was measured. Finally, knowing distance and delay time, the pressure wave velocity was calculated. Next,

by repeating this procedure, and putting accelerometers 0.4 m apart from each other in the horizontal direction, shear wave velocity of the soil medium was measured. These tests were repeated several times to minimize potential errors, with pressure and shear wave velocity being calculated as 116 m/s and 54 m/s, respectively. The physical properties of Babolsar sand, e.g. shear modulus, elastic modulus, and Poisson's ratio can be discovered from shear and pressure wave velocities. The specific gravity of the sandy soil was obtained by knowing the maximum and minimum of the dry soil unit weight and relative unit weight of the model. The mentioned parameters have been determined from the classical theory of elasticity and measured shear and pressure wave velocity, V_S , and V_P . The physical properties of Babolsar sand are reported in Table 4.

{Insert Table 4}

Gazetas [4] as well as Gazetas and Stokoe [58] suggested equations for computing the horizontal static stiffness (k_h) of the soil-foundation system. For the case of the rigid base, k_h was determined from Equation 1; similarly, Equation 2 was used to calculate the horizontal static stiffness of a homogeneous half-space model. The estimated horizontal static stiffnesses are listed in Table 5.

$$k_h = \frac{8GR}{2-\nu} \left(1 + \frac{R}{2H}\right), H/R \gg 1 \quad (1)$$

$$k_h = \frac{9GB}{2-\nu} \quad (2)$$

{Insert Table 5}

4. Basic relations

The foundation response to the dynamic loading can be obtained by considering a soil-foundation system. In the case of foundation vibration, displacement proportional to vibration will occur in the soil. Some important factors can determine the impedance function in the soil-foundation system and be found in three categories: i) soil properties such as stiffness,

unit weight, and layer thickness; secondi) foundation parameters such as shape, dimension, and hardness. Nevertheless, the most important factor in determining the impedance function is the loading frequency. For each harmonic excitation with the frequency of ω , **IFs** can be represented by a spring and damper model. By assuming a harmonic loading, $F(t) = F_0 \sin(i\omega t)$, the soil-foundation response is $x(t) = x_0 \sin(i\omega t)$, and the steady-state response of the 1-dof oscillator to the harmonic loading can be obtained by Equation 3:

$$m\ddot{x}(t) + c\dot{x}(t) + kx(t) = F(t) \quad (3)$$

By considering $x(t) = x_0 \sin(i\omega t)$, it is concluded that, $\dot{x}(t) = i\omega x_0 \cos(i\omega t)$ and $\ddot{x}(t) = -\omega^2 x_0 \sin(i\omega t)$. Finally:

$$(k - m\omega^2) + iC\omega = \frac{F(t)}{x(t)} \quad (4)$$

Given that for each particular harmonic excitation with the frequency ω , the dynamic impedance is defined as the ratio between the steady-state force (or moment) and the resulting displacement (or rotation) at the base of the massless foundation [4], based on Equation 4, the definition of a dynamic impedance function for the 1-dof system is:

$$K = (k - m\omega^2) + iC\omega \quad (5)$$

Two parts of Equation 5 are functions of the vibrational frequency, ω . The first component indicates the stiffness and inertia of the soil model. As soil properties are independent of the vibration frequency, its dependence on frequency is associated with the influence the frequency has on inertia. The second component represents the radiation and material damping of the soil-foundation system. The radiation is a result of energy dissipation by waves propagating away from the foundation, which is frequency-dependent. On the other hand, soil damping, resulting mainly from the hysteretic cyclic behavior of soil, is practically frequency independent [4].

The system with one degree of freedom, oscillator and massless soil-foundation system, Equation 5 can be rewritten as:

$$K = k_s \cdot \{k + ia_0c\} \quad (6)$$

Which a_0 is defined as $a_0 = \omega B \mathcal{N}_s$. In this study, the results are given in the form of figures that include parameters k and c with **DF**, a_0 [4].

A dynamic horizontal loading to the soil-foundation medium will appear in a horizontal force and rotation on the foundation surface. The two degrees of freedom of motion will result in four impedance equations, i.e. horizontal, rotation, rotation combined with horizontal, and horizontal combined with rotation. This approach is problematic since only two independent responses, i.e. horizontal sliding and rotation, can be measured, while four unknown impedances are to be determined. In this research, to solve the problem, the following method is used [3]. By assuming that coupled impedances are negligible, the horizontal impedance can be calculated using Equation 7:

$$S_h = \frac{F_s}{U_h} \quad (7)$$

For calculating the F_s , it is necessary to consider changes in the sliding force due to the foundation rotation and any structure attached to the foundation. So, it can be computed by Equation 8:

$$F_s = F_T + \omega^2 (M_0 U_b - M_0 b_2 \phi_b) + \omega^2 [1]^T [M] \{U\} \quad (8)$$

The first part of Equation 8 describes the horizontal force exerted to the column (F_T), the second part shows the foundation movement, and the third part considers the structural effect on the foundation. When calculating this effect, the structure is separated to individual points, each with mass properties. This separation is done as the column and frame may not be considered rigid. Each point is employed as a point that will move a unique magnitude and impart a force on the foundation. Regarding the column as rigid, the third part of Equation 8 can be assumed zero. Therefore:

$$F_s = F_T + \omega^2 (M_0 U_b - M_0 b_2 \phi_b) \quad (9)$$

So, horizontal impedance can be obtained by Equation 10:

$$S_h = \frac{F_T + \omega^2(M_0U_b - M_0b_2\phi_b)}{U_h} \quad (10)$$

On the other hand, Equation 11 and Equation 12 are used to calculate U_h and Φ_b :

$$U_h = U_b - 2b_2\phi_b \quad (11)$$

$$\phi_b = \frac{V_1 + V_2}{2B} \quad (12)$$

In this paper, the contact between the column to footing was considered rigid and attached through bolts together. Thus, Equation 10 was used to calculate the horizontal **IFs**.

Finally, the principal stages of the calculated impedance function are as follows:

- i) Logging data obtained from load cell and accelerometers,
- ii) Subtracting the average value of each series from its associated data,
- iii) Converting data to physically significant values through calibration coefficients of sensors,
- iv) Filtering acceleration data and integrating them to obtain velocity,
- v) Filtering velocity data and integrating them to obtain displacement,
- vi) Calculation of Fourier series of data and converting time domain data into the frequency domain,
- vii) Calculating the impedance functions by relevant equations (Equations 10-12).

Accordingly, by knowing the vibration frequency of each series of data, the Band-Pass Filter (BPF) technique was used. This filter permits frequencies inside a specified range to pass while the frequencies outside the range are mitigated.

5. Experimental results

The test programs for two different conditions, rigid base and half-spaced model, are presented in Table 6. The test program was designed such that minimum disturbance occurred in the soil-foundation system. In these experiments, influential parameters including footing shape, embedment ratio, footing inertia, dynamic loading domain, and dynamic

moment amplitude were chosen to examine their influence on **IFs**. Also, it should be noted that some other specifics, e.g., soil saturation degree, density or construction disturbance effect, can significantly affect the horizontal impedance functions [67]. So, the parameters mentioned above and similar ones should be considered in determining the IFs of the soil-foundation systems.

{Insert Table 6}

5.1. Effect of embedment ratio

Rigid base condition: In square footing, the dynamic stiffness coefficient of the square footing grows with the increase in the embedment ratio at $a_0 \leq 2.5$ (Figure 5-a). The dynamic stiffness at the embedment ratios 0 and 0.5 showed a similar trend, especially from a lower frequency range to moderate frequency range $a_0 \leq 2.5$. Meanwhile, at the ratio $D/h = 1$, the dynamic stiffness fluctuations were observed at a lower frequency, $a_0 = 2$. This fluctuation at $D/h=1$ may be due to the effects of the sharp edges of square footing affecting the wave propagation into the soil. Further, upon elevation of the buried ratio, the distance between the bed of the square foundation and the rigid bed decreases (60 cm to 50 cm). Distance reduction can cause higher level reflection, which has a significant effect on the results. Also, in the square footing, dynamic damping coefficients grow with the rise in the embedment ratio up to one at the lower frequency range $a_0 \leq 2.5$ (Figure 5-b). At less than $a_0 \leq 2.5$, the dynamic damping of the square footing at all three embedment ratios shows the same changes.

In circular foundation, upon D/h elevation, the dynamic damping at $a_0 \leq 1.7$ is almost unchanged while at $1.7 \leq a_0 \leq 2.5$ it increases (Figure 5-c). On the other hand, the dynamic damping of the circular footing showed a similar trend, where the embedment ratio of 1 resulted in higher value than 0 and 0.5 across the entire frequency range $a_0 \leq 2.5$ (Figure 5-d). Also, by comparing the results of the circular and square footing, it is noticed that the results are more regular in the circular footing compared to the square ones. These results confirmed the general rule that a higher embedment ratio could increase the **IFs**.

In the rigid base model for circular footing, **IFs** fluctuation was observed at the range $a_0 \leq 2.5$ according to the previously reported results (Figure 6). For **DF** less than 2, elevation of H/R ratio in the rigid base model leads to higher stiffness coefficient and minor fluctuation. So, at higher H/R values, stiffness and damping coefficients progress to the half-space model behavior. Hence, by increasing the H/R , the rigid base effect on dynamic stiffness is reduced. Lesser H/R in Gazetas [4] models in front of this study indicates that by increasing H/R , the model response leads to a half-space model and the fluctuation decreased in the model.

{Insert Figure 5}

{Insert Figure 6}

Half-space condition: For the square footing, according to Figure 7-a, the increase in the embedment ratio improved the dynamic stiffness remarkably at $a_0 \leq 2.5$. However, for $D/h=0.5$, a little perturbation of the system response was observed within the frequency range of $2 \leq a_0 \leq 2.5$. Comparable to the stiffness, similar patterns have been determined for damping (Figure 7-b). So, higher embedment ratio leads to dynamic impedance towards a more considerable value in the half-space model, especially from lower **DF** to moderate range $a_0 \leq 2.5$. Figure 8 displays that the findings have a great consistency to other studies, including Mita and Luco [6], Bu and Lin [9], and Celebi et al. [14].

Further review showed that dynamic stiffness has higher values in the rigid base model compared to the half-space model at **DF** ranges from 0.7 to 1.7. As for damping, the half-space model has mostly had larger values compared to the rigid base. Also, it is clear that both the real and imaginary parts of stiffness were greatly affected by the rigid base due resonance phenomenon in the soil-foundation system.

{Insert Figure 7}

{Insert Figure 8}

5.2. Effect of footing shape

Rigid base condition: Figure 9 indicates that the dynamic stiffness of the circular and rectangular footings is virtually the same at the lower frequency values $a_0 \leq 1.7$. At upper

ranges, $1.7 \leq a_0 \leq 2.5$, circular and rectangular foundations show similar trends. Damping of circular and square footings follows relatively similar trends at the lower frequency range of $a_0 \leq 2.5$.

A high fluctuation is also observed in both real and imaginary parts of square foundations compared to the circular form. The main reason is the sharp edges of the square footing. The sharp edges compared with the smooth shape of the circle, influences the wave propagation into the soil medium. Further, wave reflection from the bedrock has a similar pattern. So, it represents a higher level of disturbance compared to the smoothly shaped footings.

The wave transmission involves more in deeper layers, which is dependent on the bedrock position, but it is dissipated more in upper than lower layers. Accordingly, the consequence is crucial to the soil-foundation system's damping compared to stiffness. In the same vein, two resonances are observed in the square and circle footing, unlike the rectangular foundation. This indicates that by increasing the L/B , the soil-foundation response becomes more balanced.

{Insert Figure 9}

5.3. Effect of footing inertia

To study the effect of the footing inertia, four equal weights were embedded into two opposite sides of the footing increasing the footing mass.

Rigid base condition: Elevation of the footing mass has had a minor effect on the dynamic stiffness and damping of soil-foundation system in all three footing shapes; square, circular and rectangular at lower frequency range of $a_0 \leq 2.5$ (Figure 10).

Half-space condition: In the half-space model, the mass increase has not have any influence on **IFs** at $a_0 \leq 2.5$ (Figure 11). The results indicated that massless foundation theory, corresponding to dynamic stiffness and damping, is approved for **DF** lower than 2.5.

{Insert Figure 10}

{Insert Figure 11}

5.4. Effect of force amplitude

Rigid base condition: The increase in the dynamic load on the three foundations have not specific effect on the system stiffness at the frequency range of $a_0 \leq 2.5$ (Figure 12). For the square footing, the stiffness decreased low by raising the force, which it can be described by the sharpening and critical edge on the square footing which deviates the wave propagations into the soil medium. Furthermore, it is seen that the rectangular foundation has a more balanced behavior than its square counterpart (Figure 12-a&e). The observed fluctuation may be explained by the footing sharp edges which deviates the wave propagations into the soil environment. As for the circular foundation, according to Figure 12-c&d, the force amplitude has a negligible effect on dynamic stiffness and damping at lower **DF** range of $a_0 \leq 2.5$. By comparing the square and circular footing results in Figure 12, it is observed that the footing of circular shape has a smoother response, as compared to the two other footing shapes. This view is supported in damping variations by doubling the amplitude force. Elevation of the dynamic load amplitude, while considering the constancy of other parameters, creates waves with higher energy levels under the same frequencies in the soil medium. As the waves reflect, more soil particles accelerate, and the dynamic damping diminishes (Figure 12-b&d&f).

{Insert Figure 12}

Half-space condition: The elevation of the dynamic load on the half-space model has not had any influence on dynamic stiffness and damping at $a_0 \leq 2.5$ (Figure 13). Comparing Figure 12-a&b, and Figure 13, it is evident that upon elevation of the dynamic force, reflection of waves with higher energy level is visible, while in the half-space model using the sawdust in the model bottom, the load increase has had no effects on the results.

{Insert Figure 13}

5.5. Effect of dynamic moment amplitude

Half-space condition: As the horizontal loading arm increased from 15 cm to 19 cm, so did the moment on the square footing. Figure 14-a&b show that elevation of the loading arm has had a negligible effect on dynamic stiffness at $a_0 \leq 2.5$. Also, it has a minor impact on the dynamic damping at $1.6 \leq a_0 \leq 2.5$. Concerning Figure 14-c&d, it is noted that upon elevation of D/h to 1, moment increasing had no effects on the dynamic stiffness. This suggests that by raising the embedment ratio, the soil-foundation system has no influence and is balanced against the moment variations.

{Insert Figure 14}

6. Conclusions

The main goal of the current study was to determine the dynamic response of surface footings by physical scale modeling. For this purpose, a systematic experimental investigation was conducted to obtain the Impedance Functions under horizontal harmonic loading conditions in sandy soils. Tests were performed in two different situations, a rigid base and a half-space model. The relative unit weight of the developed models was 54.4 %, the void ratio was 0.64, and the shear wave velocity was 54 m/s. In the rigid base model, some parameters including foundation shape, inertia, and embedment ratio were analyzed by importing the dynamic force domain. These tests were performed in DF limits of 0.3 to 2.5 and for three footing shapes: square, circular, and rectangular. Furthermore, in the semi-infinite half-space model, for a square footing, at $0.3 \leq a_0 \leq 2.5$, the effects of footing inertia, embedment ratio, force amplitude and dynamic moment amplitude were studied. The results from both cases were compared with literature data. The following conclusions can be drawn from the present study:

1. In the rigid base model, due to propagation and reflection of waves inside the soil, complex and unpredictable behaviors were observed. In this case, generally, upon elevation of the embedment ratio, dynamic stiffness and damping increased. For the rectangular

footing, compared to other foundations, greater dynamic stiffness was observed. Further, the increasing inertia had a small effect on the real and imaginary parts of **IFs**. Similarly, more force exertion had a minimal impact on the dynamic stiffness of square and rectangular footings. It was also observed that the circular footing had a smoother response, as compared to square and rectangular foundations.

2. In the homogeneous half-space model by square footing, the results revealed that the increase in the embedment ratio considerably increased the stiffness. Note that elevation of the dynamic force and inertia at the range of $a_0 \leq 2.5$ had no influence on **IFs**. On the other hand, as the buried ratio increased, the moment effect on **IFs** diminished.

Nomenclature

a_0	Dimensionless frequency
B	Footing critical dimension
b_2	Distance from the instrumentation to the gravity center of the foundation
c	Damping coefficient of system (dimensionless)
C	Damping of system
D	Embedment depth of footing
D_r	Relative unit weight
e_{ave}	Average void ratio
e_{max}	Maximum void ratio
e_{min}	Minimum void ratio
F_s	A function of the applied horizontal force and the inertia of the footing
F_T	Applied horizontal force to the column (or footing)
$F(t)$	External dynamic force
G	Shear modulus
G_s	Specific gravity
h	Footing height
H	Soil layer thickness
k	Stiffness coefficient of system (dimensionless)
k_s	Static stiffness of system
K	Impedance function
k_h	Horizontal static stiffness
L	Footing length
m	Equivalent weight
M_0	Footing weight
R	Footing radius (or equivalent radius)
S_h	Horizontal impedance
SP	Poorly graded sand
U_b	Total motion of the instrumentation measuring horizontal motion
U_h	Maximum horizontal displacement of the footing bottom interface with the soil
V_p	Pressure wave velocity
V_s	Shear wave velocity
x, \dot{x}, \ddot{x}	Displacement, velocity and acceleration of system

$[I]$	Unit matrix
$[M]$	Matrix of point masses
$\{U\}$	Maximum horizontal displacement corresponding to the matrix of point masses
ν	Poisson's ratio
ϕ_b	Maximum rotation of the footing
ω	Cyclic excitation frequency
BPF	Band-Pass Filter
DF	Dimensionless Frequency
IFs	Impedance Functions
USCS	Unified Soil Classification System

Reference

1. Pak, R. Y., and Guzina, B. B. "Dynamic characterization of vertically loaded foundations on granular soils", *Journal of geotechnical engineering*, **121**(3), pp. 274-286 (1995).
2. Ba, Z., Liang, J., Lee, V. W., and Kang, Z. "Dynamic impedance functions for a rigid strip footing resting on a multi-layered transversely isotropic saturated half-space", *Engineering Analysis with Boundary Elements*, **86**, pp. 31-44 (2018).
3. Dunn, P. W. "Comparison of cone model and measured dynamic impedance functions of shallow foundations", PhD Thesis, University of Florida, Florida, USA (2010).
4. Gazetas, G. "Analysis of machine foundation vibrations: state of the art", *International Journal of Soil Dynamics and Earthquake Engineering*, **2**(1), pp. 2-42 (1983).
5. Novak, M. "State-of-the-art in Analysis and Design of Machine Foundations", *Developments in geotechnical engineering*, **43**, pp. 171-192 (1987).
6. Mita, A., and Luco, J. E. "Impedance functions and input motions for embedded square foundations", *Journal of geotechnical engineering*, **115**(4), pp. 491-503 (1989).
7. Meek, J. W., and Wolf, J. P. "Cone models for homogeneous soil. I", *Journal of geotechnical engineering*, **118**(5), pp. 667-685 (1992).
8. Ahmad, S., and Rupani, A. "Horizontal impedance of square foundation in layered soil", *Soil Dynamics and Earthquake Engineering*, **18**(1), pp. 59-69 (1999).
9. Bu, S., and Lin, C. H. "Coupled horizontal-rocking impedance functions for embedded square foundations at high frequency factors", *Journal of earthquake engineering*, **3**(04), pp. 561-587 (1999).
10. Kim, M. K., Lim, Y. M., and Cho, W. Y. "Three dimensional dynamic response of surface foundation on layered half-space", *Engineering structures*, **23**(11), pp. 1427-1436 (2001).
11. Wolf, J. P., and Preisig, M. "Dynamic stiffness of foundation embedded in layered halfspace based on wave propagation in cones", *Earthquake engineering & structural dynamics*, **32**(7), pp. 1075-1098 (2003).
12. Pradhan, P., Baidya, D., and Ghosh, D. "Dynamic response of foundations resting on layered soil by cone model", *Soil Dynamics and Earthquake Engineering*, **24**(6), pp. 425-434 (2004).

13. Nogami, T., Al Mahbub, A., and Chen, S. "A new method for formulation of dynamic responses of shallow foundations in simple general form", *Soil Dynamics and Earthquake Engineering*, **25**(7-10), pp. 679-688 (2005).
14. Celebi, E., Fırat, S., and Çankaya, I. "The evaluation of impedance functions in the analysis of foundations vibrations using boundary element method", *Applied Mathematics and Computation*, **173**(1), pp. 636-667 (2006).
15. Celebi, E., Fırat, S., and Cankaya, I. "The effectiveness of wave barriers on the dynamic stiffness coefficients of foundations using boundary element method", *Applied mathematics and computation*, **180**(2), pp. 683-699 (2006).
16. Liou, G.-S., and Chung, I. "Impedance matrices for circular foundation embedded in layered medium", *Soil Dynamics and Earthquake Engineering*, **29**(4), pp. 677-692 (2009).
17. Tileylioglu, S., Stewart, J. P., and Nigbor, R. L. "Dynamic stiffness and damping of a shallow foundation from forced vibration of a field test structure", *Journal of Geotechnical and Geoenvironmental Engineering*, **137**(4), pp. 344-353 (2010).
18. Han, Z., Lin, G., and Li, J. "Dynamic impedance functions for arbitrary-shaped rigid foundation embedded in anisotropic multilayered soil", *Journal of Engineering Mechanics*, **141**(11), p. 04015045 (2015).
19. Seylabi, E. E., Jeong, C., and Taciroglu, E. "On numerical computation of impedance functions for rigid soil-structure interfaces embedded in heterogeneous half-spaces", *Computers and Geotechnics*, **72**, pp. 15-27 (2016).
20. Fu, J., Liang, J., and Han, B. "Impedance functions of three-dimensional rectangular foundations embedded in multi-layered half-space", *Soil Dynamics and Earthquake Engineering*, **103**, pp. 118-122. (2017).
21. Seylabi, E. E., Jeong, C., and Taciroglu, E. "Modal and nodal impedance functions for truncated semi-infinite soil domains", *Soil Dynamics and Earthquake Engineering*, **92**, pp. 192-202 (2017).
22. Li, Z.-y., Li, J.-b., and Lin, G. "Dynamic Response of Arbitrarily Shaped Foundation Embedded in Multilayered Partially Saturated Half-Space", *International Journal of Geomechanics*, **19**(11), p. 04019121 (2019).
23. Zhang, S., and Wang, P. "Dynamic Response of a Rigid Cylinder Foundation in a Poroviscoelastic Soil Layer Resting on Rigid Bedrock under a Vertical Time-Harmonic Load", *International Journal of Geomechanics*, **19**(5), p. 04019033 (2019).
24. Lind Östlund, J., Andersson, A., Ülker-Kaustell, M., and Battini, J. M. "The influence of model assumptions on the dynamic impedance functions of shallow foundations", *International Journal of Civil Engineering*, **18**(11), pp. 1315-1326 (2020).
25. Sasmal, S. K., and Pradhan, P. K. "Effect of material damping on the impedance functions of an embedded circular foundation under vertical and horizontal excitation", *Innovative Infrastructure Solutions*, **6**(1), pp. 1-11 (2021).
26. Sasmal, S. K., and Pradhan, P. K. "Sensitivity of translational impedance functions of surface foundation to the parameters of soil and applied load", *Australian Journal of Multi-Disciplinary Engineering*, **17**(1), pp. 80-90 (2021).
27. Shi, J. Y., Chen, S. S., and Chen, K. Y. "A simplified model of layered soil for analyzing vertical vibration of loaded foundations", *Structure and Infrastructure Engineering*, pp. 1-18 (2021).
28. Terzi, V. G. "Impedance functions of a strip foundation in presence of a trench", *European Journal of Environmental and Civil Engineering*, **26**(8), pp. 3509-3546 (2022).

29. Zeolla, E., Sica, S., and De Silva, F. "Dynamic impedance functions for neighbouring shallow footings", In *Geotechnical Engineering for the Preservation of Monuments and Historic Sites III*, CRC Press, pp. 883-892 (2022).
30. Gazetas, G., Fan, K., and Kaynia, A. "Dynamic response of pile groups with different configurations", *Soil Dynamics and Earthquake Engineering*, **12**(4), pp. 239-257 (1993).
31. Goit, C.S., and Saitoh, M. "Model tests and numerical analyses on horizontal impedance functions of inclined single piles embedded in cohesionless soil", *Earthquake engineering and engineering vibration*, **12**(1), pp. 143-154 (2013).
32. Goit, C. S., and Saitoh, M. "Model tests on horizontal impedance functions of fixed-head inclined pile groups under soil nonlinearity", *Journal of Geotechnical and Geoenvironmental Engineering*, **140**(6), p. 04014023 (2014).
33. Karatzia, X., and Mylonakis, G. "Horizontal stiffness and damping of piles in inhomogeneous soil", *Journal of Geotechnical and Geoenvironmental Engineering*, **143**(4), p. 04016113 (2016).
34. Anoyatis, G., and Lemnitzer, A. "Kinematic Winkler modulus for laterally-loaded piles", *Soils and Foundations*, **57**(3), pp. 453-471 (2017).
35. Fattah, M. Y., Zbar, B. S., and Mustafa, F. S "Vertical vibration capacity of a single pile in dry sand", *Marine Georesources & Geotechnology*, **35**(8), pp. 1111-1120 (2017).
36. Wang, J., Zhou, D., Ji, T., and Wang, S. "Horizontal dynamic stiffness and interaction factors of inclined piles", *International Journal of Geomechanics*, **17**(9), p. 04017075 (2017).
37. Wang, J., and Gao, Y. "Vertical impedance of a pile in layered saturated viscoelastic half-space considering radial inhomogeneity", *Soil Dynamics and Earthquake Engineering*, **112**, pp. 107-117 (2018).
38. Zhang, S., Cui, C., and Yang, G. "Vertical dynamic impedance of pile groups partially embedded in multilayered, transversely isotropic, saturated soils", *Soil Dynamics and Earthquake Engineering*, **117**, pp. 106-115 (2019).
39. Fattah, M. Y., Zabar, B. S., and Mustafa, F. S. "Effect of saturation on response of a single pile embedded in saturated sandy soil to vertical vibration", *European Journal of Environmental and Civil Engineering*, **24**(3), pp. 381-400 (2020).
40. Wang, C., Qiao, H., Wang, Y., and Du, X. "Numerical Algorithm for Dynamic Impedance of Bridge Pile-Group Foundation and Its Validation", *Algorithms*, **14**(8), p. 247 (2021).
41. Le, Y., Wang, N., Hu, W., Geng, D., Cai, Y., and Peng, Y. "Vertical dynamic impedance of a sand-filled nodular pile in saturated soil", *Ocean Engineering*, **259**, p. 112075 (2022).
42. Ye, Z., and Yong Ai, Z. "Vertical dynamic response of a pile embedded in layered transversely isotropic unsaturated soils", *Journal of Geotechnical and Geoenvironmental Engineering*, **148**(1), p. 04021169 (2022).
43. Lin, A. N., and Jennings, P. C. "Effect of embedment on foundation-soil impedances", *Journal of engineering mechanics*, **110**(7), pp. 1060-1075 (1984).
44. Cheney, J., Brown, R., Dhat, N., and Hor, O. "Modeling free-field conditions in centrifuge models", *Journal of geotechnical engineering*, **116**(9), pp. 1347-1367 (1990).
45. Fattah, M. Y., Al-Mosawi, M. J., and Al-Ameri, A. F. "Vibration response of saturated sand-foundation system", *Earthquakes and Structures*, **11**(1), pp. 83-107 (2016).
46. Fattah, M. Y., Al-Mosawi, M. J., and Al-Ameri, A. F. "Dynamic Response of Saturated Soil-Foundation System Acted upon by Vibration", *Journal of Earthquake Engineering*, **21**(7), pp. 1158-1188 (2017).

47. Amendola, C., de Silva, F., Vratsikidis, A., Pitilakis, D., Anastasiadis, A., and Silvestri, F. "Foundation impedance functions from full-scale soil-structure interaction tests", *Soil Dynamics and Earthquake Engineering*, **141**, p. 106523 (2021).
48. Lian, J., Jiang, Q., Dong, X., Zhao, Y., and Zhao, H. "Dynamic Impedance of the Wide-Shallow Bucket Foundation for Offshore Wind Turbine Using Coupled Finite-Infinite Element Method", *Energies*, **12**(22), p. 4370 (2019).
49. Zhang, H., Niu, J., Huang, N., and Yan, Q. "Theoretical and Numerical Analysis of Soil-Pipe Pile Horizontal Vibration Based on the Fractional Derivative Viscoelastic Model", *Advances in Civil Engineering* (2021).
50. Wang, P., Zhang, M., Zhang, J., Xu, H., and Du, X. "A numerical model with high-accuracy and high-efficiency for the soil dynamic impedance of pile groups under vertical vibration", In *Structures*, **45**, pp. 489-499 (2022).
51. Nii, Y. "Experimental half-space dynamic stiffness", *Journal of geotechnical engineering*, **113**(11), pp. 1359-1373 (1987).
52. Wong, H., and Luco, J. "Dynamic response of rigid foundations of arbitrary shape", *Earthquake Engineering & Structural Dynamics*, **4**(6), pp. 579-587 (1976).
53. Momeni, R., Rostami, V., and Khazaei, J. "Study of physical modelling for piles", *Open Journal of Geology*, **7**(8), pp. 1160-1175 (2017).
54. Fry, Z. B. "Development and evaluation of soil bearing capacity", *Foundations of Structures: WES* (1963).
55. Dobry, R., and Gazetas, G. "Dynamic response of arbitrarily shaped foundations", *Journal of geotechnical engineering*, **112**(2), pp. 109-135 (1986).
56. Crouse, C., Hushmand, B., Luco, J. E., and Wong, H. "Foundation impedance functions: Theory versus experiment", *Journal of geotechnical engineering*, **116**(3), pp. 432-449 (1990).
57. Luco, J., and Wong, H. "Forced vibration of Lotung containment model: theory and observations", *Journal of Engineering Mechanics*, **116**(4), pp. 845-861(1990).
58. Gazetas, G., and Stokoe, K. H. "Free vibration of embedded foundations: theory versus experiment", *Journal of geotechnical engineering*, **117**(9), pp. 1382-1401(1991).
59. de Barros, F. C., and Luco, J. E. "Identification of foundation impedance functions and soil properties from vibration tests of the Hualien containment model", *Soil Dynamics and Earthquake Engineering*, **14**(4), pp. 229-248 (1995).
60. Stokoe, K., and Richart, F.E. "Dynamic response of embedded machine foundations", *Journal of Geotechnical and Geoenvironmental Engineering*, **100** (4), pp. 427-447 (1974).
61. Erden, S. M. "Influence of shape and embedment on dynamic foundation response", PhD Thesis, University of Massachusetts Amherst, USA (1974).
62. Fattah, M. Y., Salim, N. M., and Al-Shammary, W. T. "Effect of embedment depth on response of machine foundation on saturated sand", *Arabian Journal for Science and Engineering*, **40**(11), pp. 3075-3098 (2015).
63. Khan, A. H., Akbar, A., and Aziz, M. "Experimental Analysis of Deposition of Sands by Dry Pluviation Technique", *Journal of Engineering and Applied Sciences*, **30**(2), pp. 1-8 (2011).
64. Rajabnezhad, Y. "Effect of various parameters on dynamic response of shallow foundations by physical model tests", MSc Thesis, Sharif University of Technology, Iran (2008).

65. Stasiak, M., Molenda, M., Bańda, M., and Gondek, E. "Mechanical properties of sawdust and woodchips", *Fuel*, **159**, pp. 900-908 (2015).
66. Peres, M. A., Bono, R. W., and Brown, D. L. "Practical aspects of shaker measurements for modal testing", *Proceedings of ISMA*, pp. 2539-2550 (2010).
67. Wu, W., Yang, Z., Liu, X., Zhang, Y., Liu, H., El Naggar, M. H., Xu, M., and Mei, G. "Horizontal dynamic response of pile in unsaturated soil considering its construction disturbance effect", *Ocean Engineering*, **245**, p. 110483 (2022).

Biographies

Jafar Maleki received his B.Sc. degree in Civil Engineering from Amirkabir University of Technology and his M.Sc. in Geotechnical Engineering from Sharif University of Technology. His research orientation is towards Computational Geomechanics, Geostatistics, Soft Computing and Data Mining.

Fardin Jafarzadeh is an Associate Professor of Department of Civil Engineering, Sharif University of Technology & President of Iranian Geotechnical Society (IGS). Dr. Jafarzadeh currently teaches at the Department of Civil Engineering, Sharif University of Technology, since 1995. He does research in Soil Dynamics and Geotechnical Earthquake Engineering, Ground Improvement, Unsaturated Soil Mechanic, Earth and Rockfill Dams, Physical Modeling of Energy Piles and other fields in Geotechnical Engineering.

The results of his researches has been published in many technical journals and proceedings and presented in International conferences. He has supervised more than 60 MSc and 10 PhD students.

Tables Caption

Table 1. Babolsar sand parameters

Table 2. Sawdust parameters

Table 3. Footings dimensions

Table 4. Physical model properties

Table 5. Model static stiffness

Table 6. Tests program

Table 1. Babolsar sand parameters

e_{ave}	e_{max}	e_{min}	G_s
0.651	0.775	0.547	$\frac{2.75}{3}$

Table 2. Sawdust parameters [65]

Parameter	Unit	Value
Poured density	kN/m^3	3.1
Consolidated density	kN/m^3	7.04
Modulus of elasticity	Mpa	$0.36 \pm 0.03^*$

* In moisture content less than 10%

Table 3. Footings dimensions

Footing shape	Length (mm)	Width (mm)	Radius (mm)	Area (mm ²)	Thickness (mm)	Equivalent radius (mm)
Square	94	94	-	8836	50	53.05
Circular	-	-	53	8825	50	53
Rectangular	188	94	-	17672	50	75

Table 4. Physical model properties

Parameter	Unit	Value
Dry unit weight	kN/m ³	16.65
Pressure wave velocity	m/s	116
Shear wave velocity	m/s	54
Elastic modulus	MPa	13.2
Shear modulus	MPa	4.8
Poisson's ratio	-	0.36

Table 5. Model static stiffness

Model condition	Footing shape	Embedded ratio (D/h)	Horizontal static stiffness (k _h) (kN/m)
Rigid base condition	Square	0	1330
		0.5	1327
		1	1324

		0	1294
	Circular	0.5	1291
		1	1288
	Rectangular	0	1874
Homogeneous half-space	Square	0, 0.5, 1	1259

Table 6. Tests program

Model condition	Test number	Footing shape	Embedment ratio (D/h)	Dynamic horizontal force applied to the column (F_T) (N)	Footing mass (kg)	Loading height (cm)
Rigid base	1	square	0	10	2.4	15
	2	square	0.5	10	2.4	15
	3	square	1	10	2.4	15
	4	circular	0	10	2.6	15
	5	circular	0.5	10	2.6	15
	6	circular	1	10	2.6	15
	7	rectangular	0	10	3.3	15
	8	rectangular	0	10	4.4	15
	9	rectangular	0	20	3.3	15
	10	square	1	10	3.5	15
	11	square	1	20	2.4	15
	12	circular	1	10	3.7	15
	13	circular	1	20	2.6	15
Homogeneous Half-space	14	square	0	10	2.4	15
	15	square	0.5	10	2.4	15
	16	square	1	10	2.4	15
	17	square	1	10	3.5	15
	18	square	1	20	3.5	15

19	square	0	10	2.4	19
20	square	1	10	2.4	19

Figures Caption

Figure 1. Particle size distribution for Babolsar sand

Figure 2. Results of sand raining calibration test

Figure 3. Connection details of column and square footing, a) XZ view, and b) YZ view (mm)

Figure 4. Physical model overview

Figure 5. Comparison of the effect of embedded ratio to dynamic stiffness and damping in rigid base model, a) Real part of square footing, b) Imaginary part of square footing, c) Real part of circular footing, and d) Imaginary part of circular footing

Figure 6. Comparison of the results of this study in rigid base condition with Gazetas (1983), a) Real part, and b) Imaginary part

Figure 7. Comparison of the effect of embedded ratio to dynamic stiffness and damping for square footing in half-space model, a) Real part, and b) Imaginary part

Figure 8. Comparison of the results of this study in half-space condition with other researchers (Mita & Luco (1989), Bu & Lin (1999) and Celebi et al., (2006a))

Figure 9. Comparison of the effect of footing shape to the dynamic stiffness and damping in the rigid base model, a) Real part, and b) Imaginary part

Figure 10. Comparison of the effect of footing inertia to dynamic stiffness and damping in the rigid base model, a) Real part of square footing, b) Imaginary part of square footing, c) Real part of circular footing, d) Imaginary part of circular footing, e) Real part of rectangular footing, and f) Imaginary part of rectangular footing

Figure 11. Comparison of the effect of footing inertia to dynamic stiffness and damping for square footing in half-space model, a) Real part, and b) Imaginary part

Figure 12. Comparison of the effect of force magnitude to dynamic stiffness and damping in the rigid base model, a) Real part of square footing, b) Imaginary part of square footing, c) Real part of circular footing, d) Imaginary part of circular footing, e) Real part of rectangular footing, and f) Imaginary part of rectangular footing

Figure 13. Comparison of the effect of force magnitude to dynamic stiffness and damping for square footing in half-space model, a) Real part, and b) Imaginary part

Figure 14. Comparison of the effect of loading arm to dynamic stiffness and damping for square footing in half-space model, a) Real part at $D/h=0$, b) Imaginary part at $D/h=0$, c) Real part at $D/h=1$, and d) Imaginary part at $D/h=1$

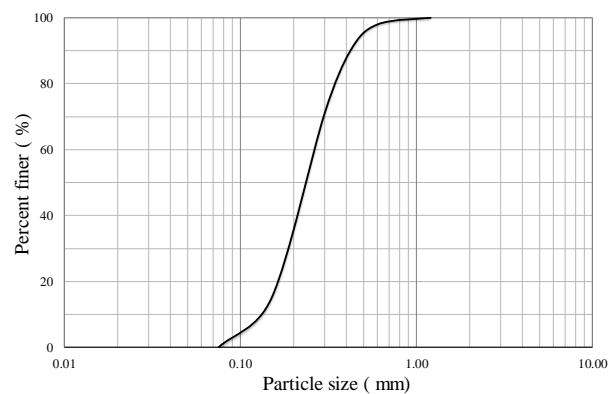


Figure 1. Particle size distribution for Babolsar sand

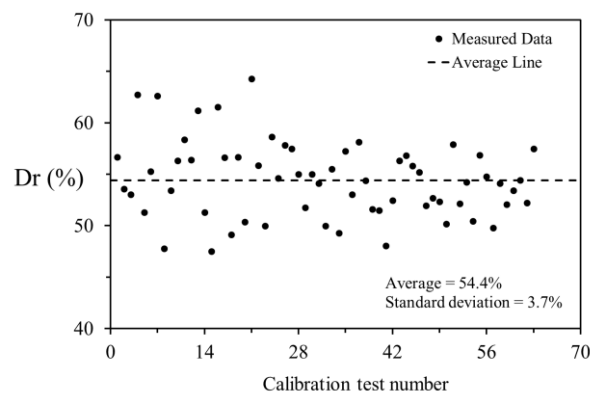


Figure 2. Results of sand raining calibration test

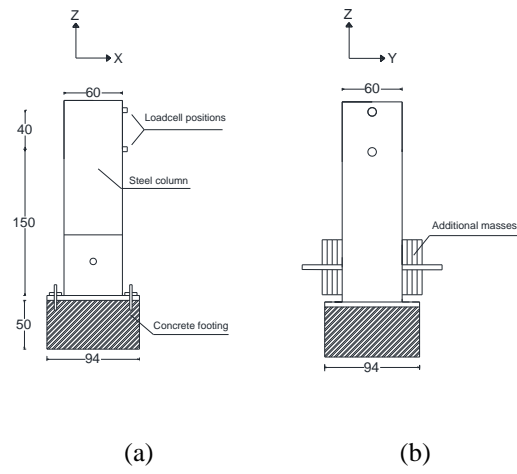


Figure 3. Connection details of column and square footing, a) XZ view, and b) YZ view (mm)

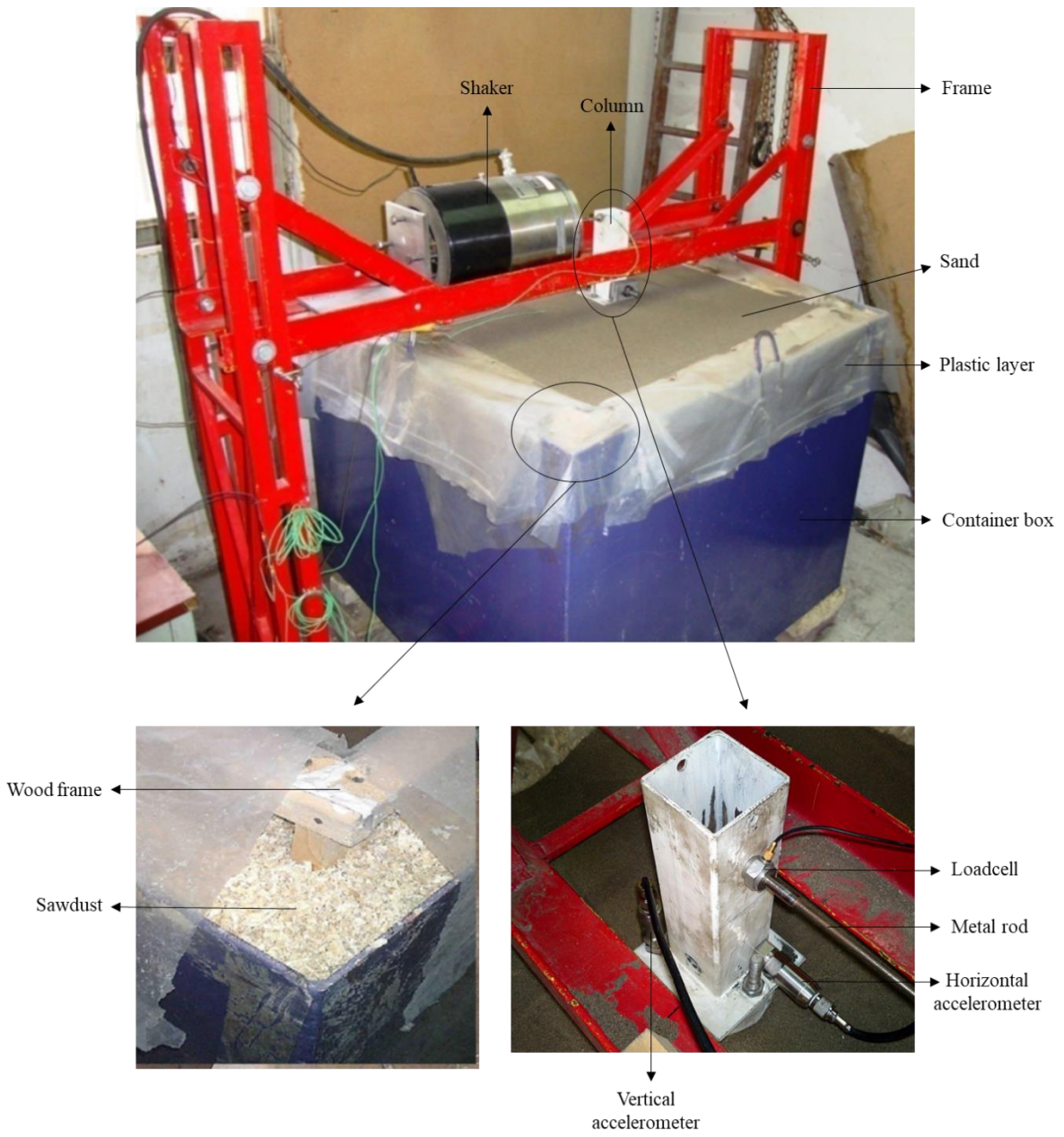


Figure 4. Physical model overview

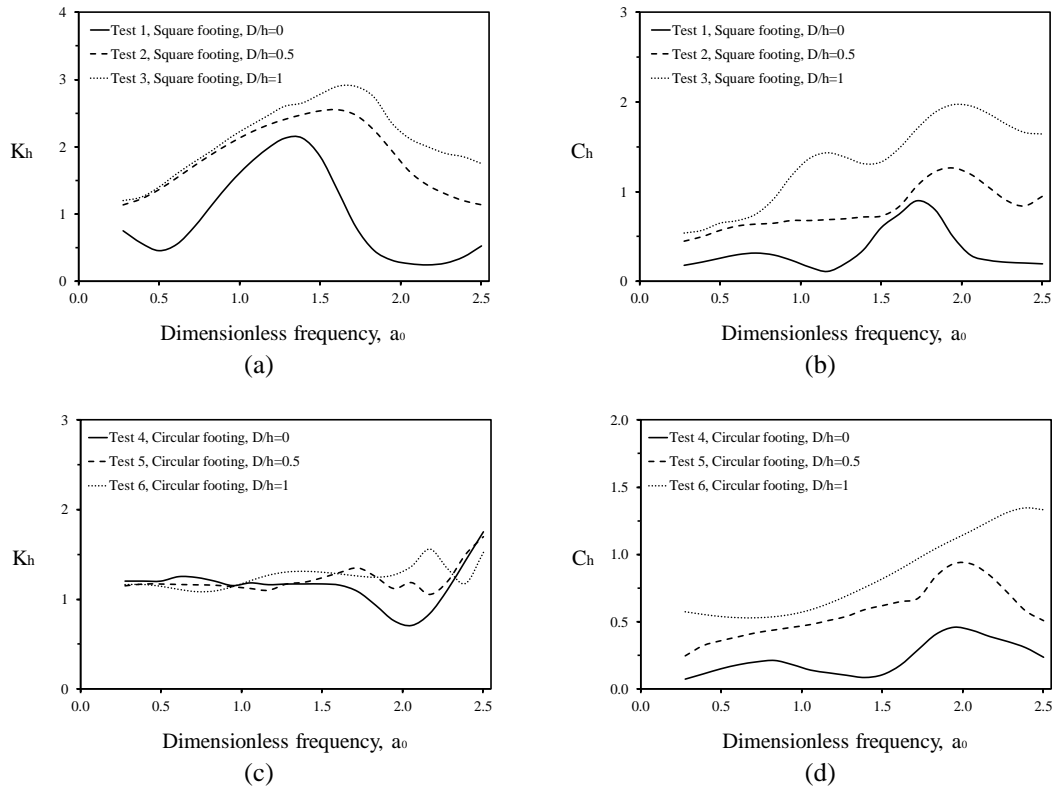


Figure 5. Comparison of the effect of embedded ratio to dynamic stiffness and damping in rigid base model, a) Real part of square footing, b) Imaginary part of square footing, c) Real part of circular footing, and d) Imaginary part of circular footing

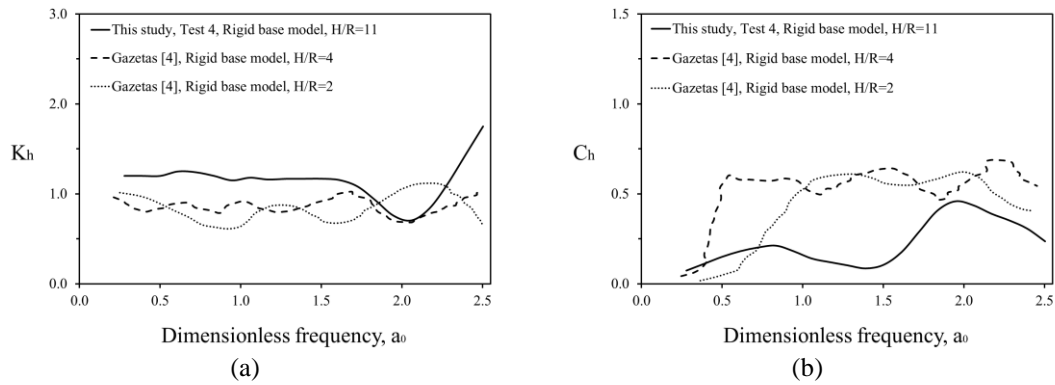


Figure 6. Comparison of the results of this study in rigid base condition with Gazetas [4], a) Real part, and b) Imaginary part

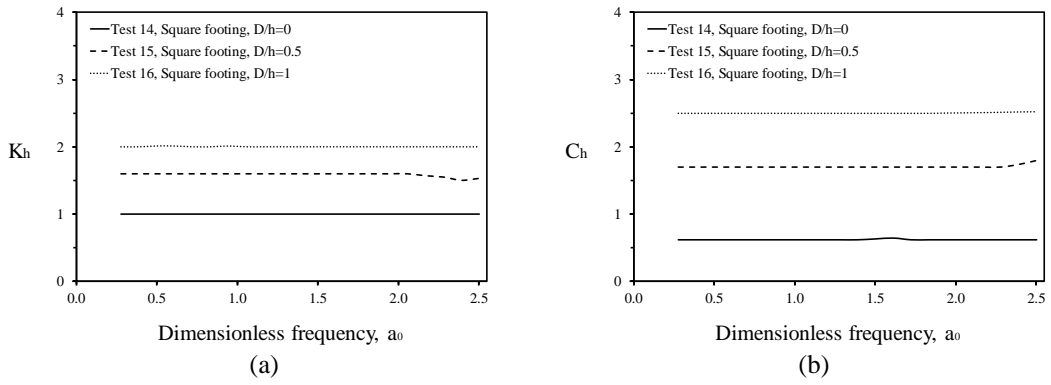


Figure 7. Comparison of the effect of embedded ratio to dynamic stiffness and damping for square footing in half-space model, a) Real part, and b) Imaginary part

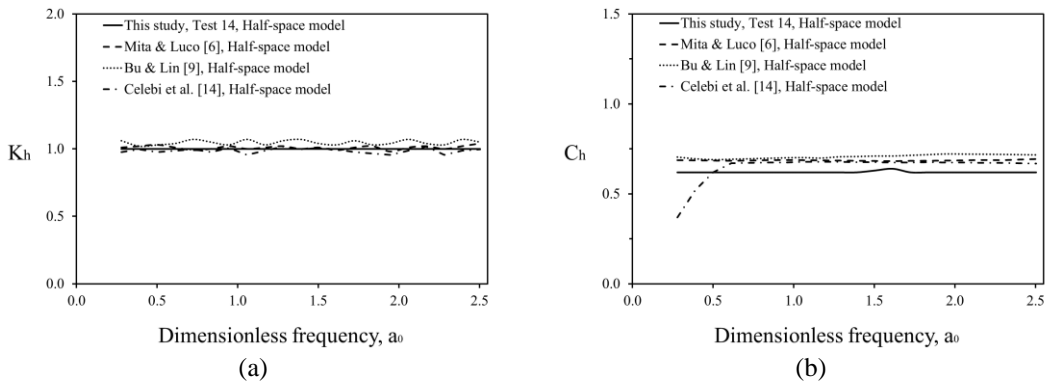


Figure 8. Comparison of the results of this study in half-space condition with other researchers (Mita & Luco [6], Bu & Lin [9], and Celebi et al. [14])

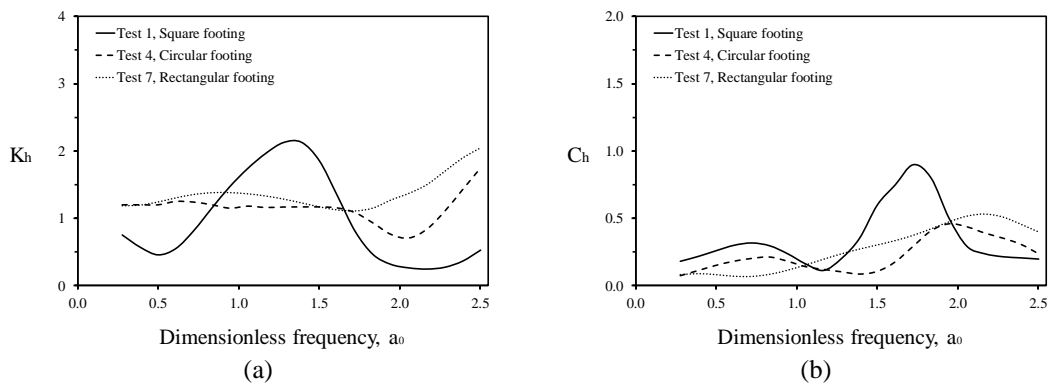


Figure 9. Comparison of the effect of footing shape to the dynamic stiffness and damping in the rigid base model, a) Real part, and b) Imaginary part

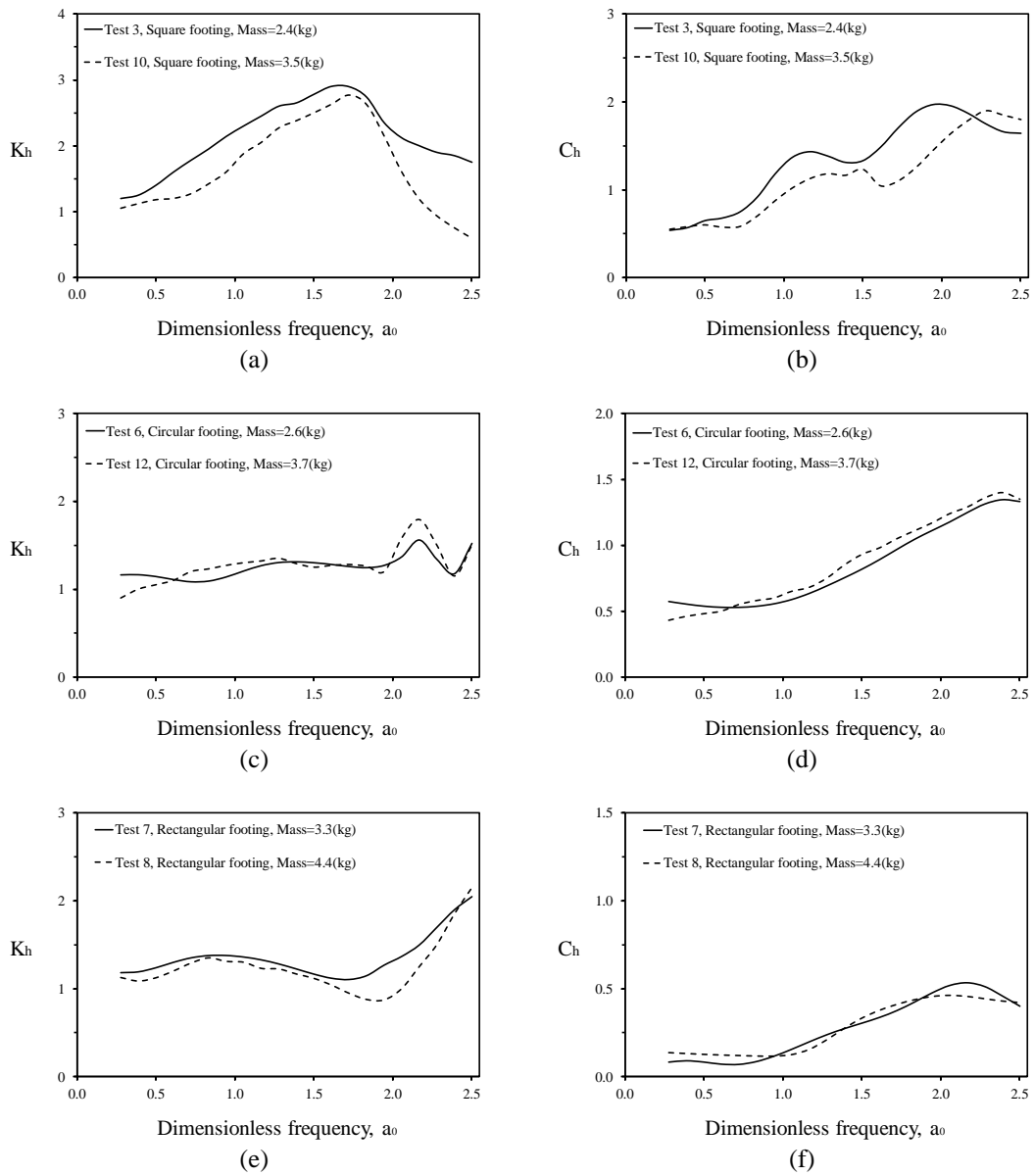


Figure 10. Comparison of the effect of footing inertia to dynamic stiffness and damping in the rigid base model, a) Real part of square footing, b) Imaginary part of square footing, c) Real part of circular footing, d) Imaginary part of circular footing, e) Real part of rectangular footing, and f) Imaginary part of rectangular footing

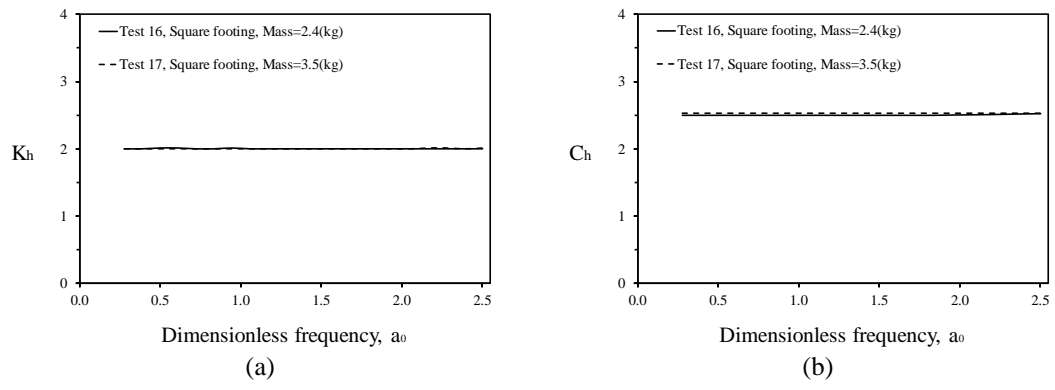


Figure 11. Comparison of the effect of footing inertia to dynamic stiffness and damping for square footing in half-space model, a) Real part, and b) Imaginary part

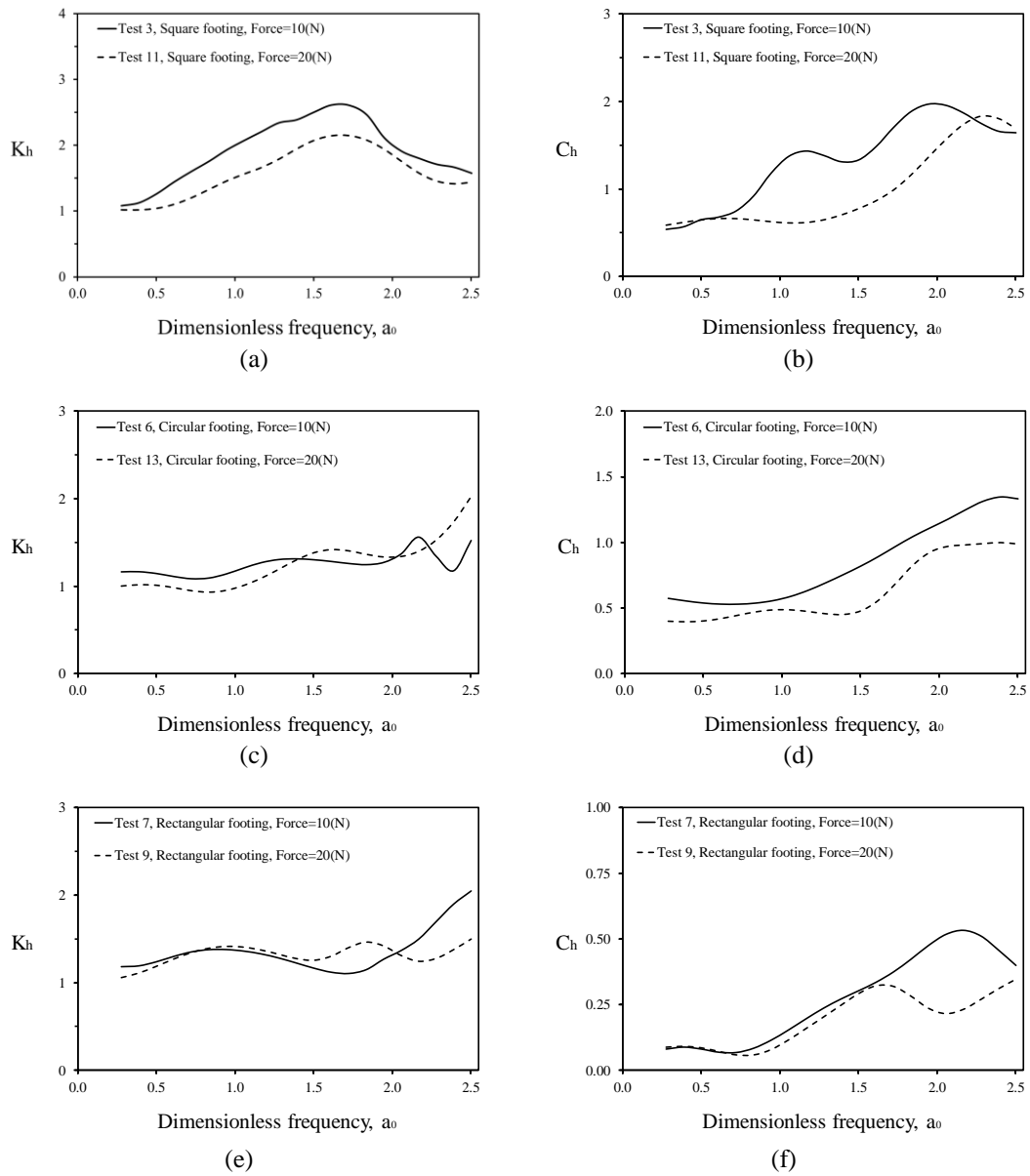


Figure 12. Comparison of the effect of force magnitude to dynamic stiffness and damping in the rigid base model, a) Real part of square footing, b) Imaginary part of square footing, c) Real part of circular footing, d) Imaginary part of circular footing, e) Real part of rectangular footing, and f) Imaginary part of rectangular footing

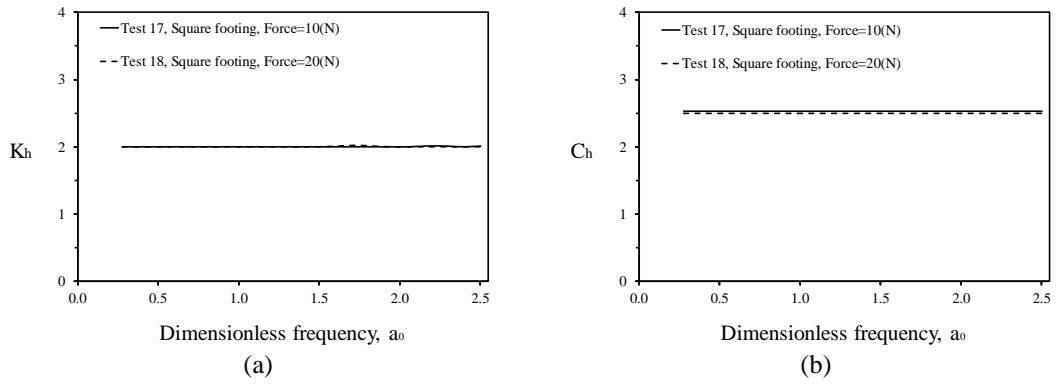


Figure 13. Comparison of the effect of force magnitude to dynamic stiffness and damping for square footing in half-space model, a) Real part, and b) Imaginary part

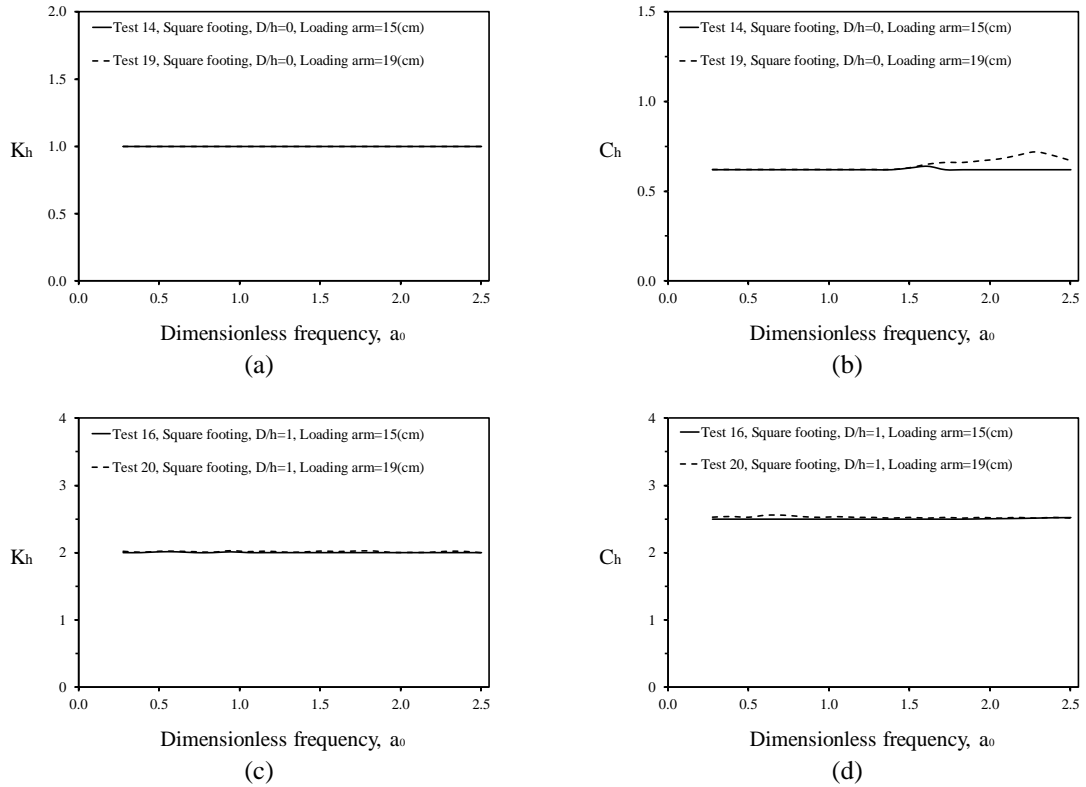


Figure 14. Comparison of the effect of loading arm to dynamic stiffness and damping for square footing in half-space model, a) Real part at $D/h=0$, b) Imaginary part at $D/h=0$, c) Real part at $D/h=1$, and d) Imaginary part at $D/h=1$